Springer

Journal of
Mechanical
Science and
Technology

Journal of Mechanical Science and Technology 22 (2008) 1058~1072

www.springerlink.com/content/1738-494x

Analytical investigation on axisymmetric free vibrations of moderately thick circular functionally graded plate integrated with piezoelectric layers

F. Ebrahimi[1,2], A. Rastgoo[1,*] and M.H.Kargarnovin[3]

[1]*Department of Mechanical Engineering, University of Tehran, Tehran, Iran*

[2]*Mechanical Engineering Department, Faculty of Engineering and Technology, Imam Khomeini International University, Qazvin, Iran*

[3]*Department of Mechanical Engineering, Sharif University of Technology, Tehran, Iran*

(Manuscript Received August 27, 2007; Revised December 22, 2007; Accepted March 6, 2008)

Abstract

In this paper, a free vibration analysis of moderately thick circular functionally graded (FG) plate integrated with two thin piezoelectric (PZT4) layers is presented based on Mindlin plate theory. The material properties of the FG core plate are assumed to be graded in the thickness direction, while the distribution of electric potential field along the thickness of piezoelectric layers is simulated by sinusoidal function. The differential equations of motion are solved analytically for two boundary conditions of the plate: clamped edge and simply supported edge. The analytical solution is validated by comparing the obtained resonant frequencies with those of an isotropic host plate. The emphasis is placed on investigating the effect of varying the gradient index of FG plate on the free vibration characteristics of the structure. Good agreement between the results of this paper and those of the finite element analyses validated the presented approach.

Keywords: Functionally graded; Piezoelectric; Circular plate; Free vibration; Mindlin plate theory

1. Introduction

A new class of materials known as 'functionally graded materials' (FGMs) has emerged recently, in which the material properties vary continuously throughout the continuum and specifically in the plates along the thickness direction. In an effort to develop the super heat-resistant materials, Koizumi [1] first proposed the concept of FGM. These materials are microscopically heterogeneous and are typically made from isotropic components, such as metals and ceramics.

The laminated composite structures can be tailored to design advanced structures, but the sharp change in the properties of each layer at the interface between two adjacent layers causes large interlaminar shear stresses that may eventually give rise to the well known phenomenon known as delamination. Such detrimental effects can be mitigated by grading the properties in a continuous manner across the thickness direction. For example, Teymur et al. [2] carried out a thermo-mechanical analysis of materials, which are functionally graded in two directions, and demonstrated that the onset of delamination could be prevented by tailoring the microstructures of the composite piles. Thus, the use of FGM may become an important issue for developing advanced structures. Intensive research has already been reported on the buckling analysis [3], dynamic analysis [4], and nonlinear thermo-elastic analysis of structures made of FGM [5].

In the quest for developing lightweight, high performing flexible structures, a concept emerged to develop structures with self-controlling and self-monitoring capabilities. Expediently, these capabilities of a structure were achieved by exploiting the converse and direct innate effects of the piezoelectric materials as distributed actuators or sensors, which are mounted or embedded in the structure [6]. Such

*Corresponding author. Tel.: +98 21 8800 5677, Fax.: +98 21 8801 3029
E-mail address: arastgo@ut.ac.ir
DOI 10.1007/s12206-008-0303-2

structures having built-in mechanisms for achieving self-controlling and/or self-monitoring capabilities are customarily known as 'smart structures'. The concept of developing smart structures has been extensively used for active control of flexible structures during the past decade [7]. In this regard, the use of axisymmetric piezoelectric actuators in the form of a disc or ring to produce motion in a circular or annular substrate plate is common in a wide range of applications including micro-pumps and micro-valves [8, 9] devices for generating and detecting sound [10], and implantable medical devices [11]. They may also be useful in other applications such as microwave microswitches where it is important to control distortion due to intrinsic stresses [12].

Recently, considerable interest has also been focused on investigating the performance of FG plates integrated with piezoelectric actuators. For example, Ootao & Tanigawa [13] theoretically investigated the simply supported FG rectangular plate integrated with a piezoelectric plate subjected to transient thermal loading. A 3-D solution for rectangular FG plates coupled with a piezoelectric actuator layer was proposed by Reddy & Cheng [14] using transfer matrix and asymptotic expansion techniques. Wang & Noda [15] analyzed a smart FG composite structure composed of a layer of metal, a layer of piezoelectric and an FG layer in between, while in [16] a finite element model was developed for studying the shape and vibration control of FG plates integrated with piezoelectric sensors and actuators. Yang et al. [17] investigated the nonlinear thermo-electro-mechanical bending response of FG rectangular plates that are covered with monolithic piezoelectric actuator layers on the top and bottom surfaces of the plate. They [18] also presented a large amplitude vibration analysis of a rectangular FG plate with surface-bonded piezoelectric layers by using a semi-analytical method based on 1D differential quadrature and Galerkin technique. Most recently, Huang & Shen [19] investigated the dynamics of an FG plate coupled with two monolithic piezoelectric layers at its top and bottom surfaces undergoing nonlinear vibrations in thermal environments. All the aforementioned studies focused on the rectangular-shaped plate structures.

However, to the authors' best knowledge, no researches dealing with the free vibration characteristics of the circular FGM plate integrated with the piezoelectric layers have been reported. Therefore, in conjunction with our recent works [20, 21], we attempt to solve this problem, that is, to provide an analytical solution for free vibration of moderately thick circular FG plates with two full-sized surface-bonded piezoelectric layers on the top and the bottom of the FG plate (see Fig. (1)). The formulations are based on first order shear deformation plate theory (FSDPT). A consistent formulation that satisfies the Maxwell static electricity equation is presented so that the full coupling effect of the piezoelectric layer on the dynamic characteristics of the circular FGM plate can be estimated based on the free vibration results. The physical and mechanical properties of the FG core plate are assumed to be graded continuously in the thickness direction according to the power-law distribution in terms of the volume fractions of the constituents, whereas the distribution of electric potential field along the thickness direction of piezoelectric layers is simulated by a sinusoidal function. The differential equations of motion are solved analytically for clamped edge and simply supported edge boundary condition of the plate. By use of some mathematical techniques these differential equations are transformed to a sixth order ordinary differential equation, and finally by implementing the operator decomposition method on this equation, three Bessel types of equations are obtained which can easily be solved for the plate deflection, plate rotation, and consequently the potential function. The detailed mathematical derivations are presented. Numerical investigations are performed for FG plates with two surface-bonded piezoelectric layers for various piezo-layer thicknesses. Emphasis is also placed on investigating the effect of varying the gradient index of FG plate on the free vibration characteristics of the structure. For some specific cases, obtained results were cross checked with the existing literature and, furthermore, verified by those obtained from three-dimensional finite element analyses.

2. FG and piezoelectric materials

2.1. Functionally graded materials (FGM)

Several available analytical and computational models have discussed the issue of finding suitable functions for the material properties, and there are several criteria for selecting them. They are desired to be continuous, simple and should have the ability to exhibit curvature, both ''concave upward'' and ''concave downward'' [22]. In this study the simple power

law, which has all the desired properties, is used. Nowadays not only can FGM easily be produced, but one can control even the variation of the FG constituents in a specific way. For example, in an FG material made of ceramic and metal mixture, we have;

$$V_m + V_c = 1 \tag{1}$$

In which V_c and V_m are the volume fraction of the ceramic and metallic part, respectively. Based on the power law distribution [23], the variation of V_c vs. thickness coordinate (z) with its origin placed at the middle of thickness, can be expressed as:

$$V_c = (z/2h_f + 1/2)^g \ , g \geq 0 \ , \tag{2}$$

in which $2h_f$ is the FG core plate thickness, g is the FGM Volume fraction index (see Fig. (1)).

Note that the variation of both constituents of ceramics and metal is linear when $g=1$. Moreover, for $g=0$, a fully ceramic plate is intended. All other mechanical, physical and thermal properties of FGM media follow the same distribution as for V_c. We assume that the inhomogeneous material properties, such as the modulus of elasticity E and the density ρ change within the thickness direction z based on Voigt's rule over the whole range of the volume fraction [24] as follows; while the Poisson ratio υ is assumed to be constant in the thickness direction [25] as:

$$\begin{aligned} E(z) &= (E_c - E_m)V_c(z) + E_m \\ \rho(z) &= (\rho_c - \rho_m)V_c(z) + \rho_m \\ \nu(z) &= \nu \end{aligned} \tag{3}$$

where subscripts m and c refer to the metal and ceramic constituents, respectively. After substituting V_c from Eq. (2) into Eqs. (3), material properties of the FGM plate are determined in the power law form which are the same as those proposed by Reddy & Praveen [23]:

$$\begin{aligned} E(z) &= (E_c - E_m)(z/2h_f + 1/2)^g + E_m \\ \rho(z) &= (\rho_c - \rho_m)(z/2h_f + 1/2)^g + \rho_m \end{aligned} \tag{4}$$

2.2. Piezoelectric materials

A constitutive 2D elasto-static relation for symmetry piezoelectric materials in Cartesian coordinates is given as follows [26]:

$$\sigma_i = C_{ki}\varepsilon_k - e_{ji}E_k \quad i,j,k = 1,2,3 \tag{5}$$

Based on well-known assumptions of FSDPT, Eq. (5) can be represented by [27]:

$$\begin{pmatrix} \sigma_{11} \\ \sigma_{22} \\ \sigma_{12} \\ \sigma_{13} \\ \sigma_{23} \end{pmatrix} = \begin{pmatrix} \bar{C}_{11}^E & \bar{C}_{12}^E & 0 & 0 & 0 \\ \bar{C}_{12}^E & \bar{C}_{11}^E & 0 & 0 & 0 \\ 0 & 0 & (\bar{C}_{11}^E - \bar{C}_{12}^E)/2 & 0 & 0 \\ 0 & 0 & 0 & C_{55}^E & 0 \\ 0 & 0 & 0 & 0 & C_{55}^E \end{pmatrix} \begin{pmatrix} \varepsilon_{11} \\ \varepsilon_{22} \\ \gamma_{12} \\ \gamma_{13} \\ \gamma_{23} \end{pmatrix} - \begin{pmatrix} 0 & 0 & \bar{e}_3 \\ 0 & 0 & \bar{e}_{31} \\ 0 & 0 & 0 \\ e_{15} & 0 & 0 \\ 0 & e_{15} & 0 \end{pmatrix} \begin{pmatrix} E_1 \\ E_2 \\ E_3 \end{pmatrix} \tag{6}$$

in which σ_i and ε_k represent the stress and strain components, respectively, and e represents the permeability constant of piezoelectric material and E_k indicates the components of the electric field. Also, c_{ij} is related to the matrix of modulus of elasticity, and $\bar{C}_{ij}^E$ are the components of the symmetric piezoelectric stiffness matrix given as follows, and $\bar{e}_{31}$ is the reduced permeability constant of piezoelectric material and given as [28]:

$$\begin{aligned} &\bar{C}_{11}^E = C_{11}^E - \left(C_{13}^E\right)^2 / C_{33}^E \qquad \bar{C}_{12}^E = C_{12}^E - \left(C_{13}^E\right)^2 / C_{33}^E \\ &\bar{e}_{31}^E = e_{31} - C_{13}^E e_{33} / C_{33}^E \end{aligned}$$

Moreover, the electric displacement-strain relation for the piezoelectric material is given by [26]:

$$\begin{pmatrix} D_1 \\ D_2 \\ D_3 \end{pmatrix} = \begin{pmatrix} 0 & 0 & 0 & e_{15} & 0 \\ 0 & 0 & 0 & 0 & e_{15} \\ \bar{e}_{31} & \bar{e}_{31} & 0 & 0 & 0 \end{pmatrix} \{\varepsilon_{11}\ \varepsilon_{22}\ \gamma_{12}\ \gamma_{13}\ \gamma_{23}\}^T + \begin{pmatrix} \bar{\Xi}_{11} & 0 & 0 \\ 0 & \bar{\Xi}_{11} & 0 \\ 0 & 0 & \bar{\Xi}_{33} \end{pmatrix} \begin{Bmatrix} E_1 \\ E_2 \\ E_3 \end{Bmatrix} \tag{7}$$

in which D_i (i=1,2,3) represents the components of an electric displacement, $\bar{\Xi}_{11}$, $\bar{\Xi}_{33}$ are the symmetric reduced dielectric constants of piezoelectric layer and given as [28]:

$$\bar{\Xi}_{33} = \bar{\Xi}_{33} + (e_{33}^2 / C_{33}^E) \quad \bar{\Xi}_{11} = \Xi_{11}$$

in which Ξ_{33} , Ξ_{11} are the dielectric constants (permittivity).

3. Constitutive relations for an FG plate and piezoelectric layers under an electric potential field

3.1 FSDPT based strain and stress field in circular FGM plate

Usually, in the analysis of thick circular plate, the first order shear deformation plate theory is used in which the effect of the shear deformation and the rotary inertia cannot be omitted. It is assumed that (a) there is no "thickness stretch" of the plate, and (b) straight material lines that are perpendicular to the mid-plane in the undeformed state remain straight in the deformed state even though they may not remain perpendicular to the mid-plane. According to this theory, the displacement fields of the plate in the cylindrical coordinate shown in Fig. (1) are given as [29]:

$$u_z = u_z(r,\theta,z,t) = w(r,\theta,t) \tag{8}$$

$$u_r = u_r(r,\theta,z,t) = z\psi_r(r,\theta,t) \tag{9}$$

$$u_\theta = u_\theta(r,\theta,z,t) = -z\psi_\theta(r,\theta,t) \tag{10}$$

where u_z, u_r, and u_θ are the displacements of the plate in the transverse, radial, and tangential direction, respectively; w is the transverse displacement of the mid-plane; and ψ_r and ψ_θ are the rotations of vertical lines perpendicular to the mid-plane, measured on the z–r and z–θ planes, respectively.

It is also assumed that the poling direction of the piezoelectric material is in the z-direction. A differential strain can be induced in case of applying external electric potential across the piezoelectric layer resulting in bending of the plate. The strain of the FGM plate and piezoelectric layer in the radial and tangential directions and the shear component are given by [30]:

$$\varepsilon_{rr} = \frac{\partial u_r}{\partial r} = z\frac{\partial \psi_r}{\partial r} \tag{11}$$

$$\varepsilon_{\theta\theta} = \frac{\partial u_\theta}{r\partial\theta} + \frac{u_r}{r} = z\left(\frac{\partial \psi_\theta}{r\partial\theta} + \frac{\psi_r}{r}\right) \tag{12}$$

$$\gamma_{r\theta} = \frac{\partial u_r}{r\partial\theta} + \frac{\partial u_\theta}{\partial r} - \frac{u_\theta}{r} = z\left(\frac{\partial \psi_r}{r\partial\theta} - \frac{\psi_\theta}{r} + \frac{\partial \psi_\theta}{\partial r}\right) \tag{13}$$

$$\gamma_{rz} = \frac{\partial u_r}{\partial z} + \frac{\partial u_z}{\partial r} = \psi_r + \frac{\partial w}{\partial r} \tag{14}$$

$$\gamma_{\theta z} = \frac{\partial u_\theta}{\partial z} + \frac{\partial u_z}{r\partial\theta} = \psi_\theta + \frac{\partial w}{r\partial\theta} \tag{15}$$

The stress components in the FGM plate in terms of strains or component of displacement field based on the generalized Hooke's Law are [30]:

$$\sigma_{rr}^f = \frac{E(z)}{1-\nu^2}(\varepsilon_{rr} + \nu\varepsilon_{\theta\theta}) = \frac{zE(z)}{1-\nu^2}\left[\frac{\partial \psi_r}{\partial r} + \nu\left(\frac{\partial \psi_\theta}{r\partial\theta} + \frac{\psi_r}{r}\right)\right] \tag{16}$$

$$\sigma_{\theta\theta}^f = \frac{E(z)}{1-\nu^2}(\varepsilon_{\theta\theta} + \nu\varepsilon_{rr}) = \frac{zE(z)}{1-\nu^2}\left[\frac{\psi_r}{r} + \frac{\partial \psi_\theta}{r\partial\theta} + \nu\frac{\partial \psi_r}{\partial r}\right] \tag{17}$$

$$\tau_{r\theta}^f = \frac{E(z)}{2(1+\nu)}\gamma_{r\theta} = \frac{zE(z)}{2(1+\nu)}\left[\frac{\partial \psi_\theta}{\partial r} - \frac{\psi_\theta}{r} + \frac{\partial \psi_r}{r\partial\theta}\right] \tag{18}$$

$$\tau_{rz}^f = \kappa^2\frac{E(z)}{2(1+\nu)}\gamma_{rz} = \kappa^2\frac{E(z)}{2(1+\nu)}\left[\psi_r + \frac{\partial w}{\partial r}\right] \tag{19}$$

$$\tau_{\theta z}^f = \kappa^2\frac{E(z)}{2(1+\nu)}\gamma_{\theta z} = \kappa^2\frac{E(z)}{2(1+\nu)}\left[\psi_\theta + \frac{\partial w}{r\partial\theta}\right] \tag{20}$$

where $E(z)$ the Young's modulus of the FGM material is expressed in Eq. (4) and the shear factor (κ) employed in Mindlin's plate model to correct for the shear modulus, chosen as $\pi/\sqrt{12}$ here [29]; moreover, the superscript (f) indicates the variable in the FG core plate.

3.2 The electric potential, electric intensity, flux density and strain-stress relations in the piezoelectric layers

Two piezoelectric layers are attached to the FG plate and are intended to be used as an actuator or sensor to determine the natural frequencies of a vibrating coupled plate. There are several different models representing the input electric potential for such a piezoelectric layer. In this paper we decided to adopt the following sinusoidal function for electric potential proposed by Liu et al. [31], which is appropriate for free vibrations of the proposed system:

$$\phi(r,\theta,z,t) = \begin{cases} \varphi(r,\theta,t)\sin\left(\pi(z-h_f)/h_p\right) & h_f \le z \le h_f + h_p \\ \varphi(r,\theta,t)\sin\left(\pi(-z-h_f)/h_p\right) & -h_f - h_p \le z \le -h_f \end{cases} \tag{21}$$

where, as indicated before, z is measured from the mid-plane of the plate in the transverse direction. It is to be noted that the assumed potential function satisfies the boundary condition that electric potential vanishes at the internal surfaces $z=\pm h_f$ and the exter-

nal surfaces $z=\pm(h_f+h_p)$.

Based on the assumption of electric potential distribution across the thickness direction shown in Eq. (21), the components of electric field intensity E and electric flux density D can be written in the cylindrical coordinate as [32]:

$$E_r = -\frac{\partial \phi}{\partial r} = -\frac{\partial \varphi}{\partial r}\sin\frac{\pi(z-h_f)}{h_p} \tag{22}$$

$$E_\theta = -\frac{\partial \phi}{r\partial \theta} = -\frac{\partial \varphi}{r\partial \theta}\sin\frac{\pi(z-h_f)}{h_p} \tag{23}$$

$$E_z = -\frac{\partial \phi}{\partial z} = -\frac{\pi\varphi}{h_p}\cos\frac{\pi(z-h_f)}{h_p} \tag{24}$$

$$D_r = e_{15}\gamma_{rz} + \bar{\Xi}_{11}E_r = e_{15}\left(\psi_r + \frac{\partial w}{\partial r}\right) - \bar{\Xi}_{11}\frac{\partial \varphi}{\partial r}\sin\frac{\pi(z-h_f)}{h_p} \tag{25}$$

$$D_\theta = e_{15}\gamma_{\theta z} + \bar{\Xi}_{11}E_\theta = e_{15}\left(\psi_\theta + \frac{\partial w}{r\partial \theta}\right) - \bar{\Xi}_{11}\frac{\partial \varphi}{r\partial \theta}\sin\frac{\pi(z-h_f)}{h_p} \tag{26}$$

$$\begin{aligned} D_z &= \bar{\bar{\Xi}}_{33}E_z + \bar{e}_{31}\left(\varepsilon_{rr}+\varepsilon_{\theta\theta}\right) \\ &= -\bar{\bar{\Xi}}_{33}\frac{\pi\varphi}{h_p}\cos\frac{\pi(z-h_f)}{h_p} \\ &\quad + z\bar{e}_{31}\left(\frac{\partial \psi_r}{\partial r} + \frac{\psi_r}{r} + \frac{\partial \psi_\theta}{r\partial \theta}\right) \end{aligned} \tag{27}$$

The stress-strain-electric field intensity relations in the piezoelectric layers in cylindrical coordinates referred to Eq. (6) can be written as:

$$\sigma_{rr}^p = \bar{C}_{11}^E\varepsilon_{rr} + \bar{C}_{12}^E\varepsilon_{\theta\theta} - \bar{e}_{31}E_z \tag{28}$$

$$\sigma_{\theta\theta}^p = \bar{C}_{12}^E\varepsilon_{rr} + \bar{C}_{11}^E\varepsilon_{\theta\theta} - \bar{e}_{31}E_z \tag{29}$$

$$\tau_{r\theta}^p = \frac{1}{2}\left(\bar{C}_{11}^E - \bar{C}_{12}^E\right)\gamma_{r\theta} = z\left(\bar{C}_{11}^E - \bar{C}_{12}^E\right)\left(\frac{\partial \psi_r}{r\partial \theta} - \frac{\psi_\theta}{r} + \frac{\partial \psi_\theta}{\partial r}\right) \tag{30}$$

$$\tau_{rz}^p = \kappa^2 C_{55}^E\gamma_{rz} + e_{15}E_r \tag{31}$$

$$\tau_{\theta z}^p = \kappa^2 C_{55}^E\gamma_{\theta z} + e_{15}E_\theta \tag{32}$$

4. Derivation of the governing differential equations of the piezoelectric coupled FGM circular plate

In order to obtain the governing differential equation of the coupled circular plate, we begin with resultant moments and resultant shear force components as [27]:

$$\begin{aligned} M_{rr} &= \int_{-h_f-h_p}^{h_f+h_p} z\sigma_{rr}dz = \int_{-h_f}^{h_f} z\sigma_{rr}^f dz + 2\int_{h_f}^{h_f+h_p} z\sigma_{rr}^p dz \\ M_{\theta\theta} &= \int_{-h_f-h_p}^{h_f+h_p} z\sigma_{\theta\theta}dz = \int_{-h_f}^{h_f} z\sigma_{\theta\theta}^f dz + 2\int_{h_f}^{h_f+h_p} z\sigma_{\theta\theta}^p dz \\ M_{r\theta} &= \int_{-h_f-h_p}^{h_f+h_p} z\tau_{r\theta}dz = \int_{-h_f}^{h_f} z\tau_{r\theta}^f dz + 2\int_{h_f}^{h_f+h_p} z\tau_{r\theta}^p dz \\ Q_r &= \int_{-h_f-h_p}^{h_f+h_p} \tau_{rz}dz = \int_{-h_f}^{h_f} \tau_{rz}^f dz + 2\int_{h_f}^{h_f+h_p} \tau_{rz}^p dz \\ Q_\theta &= \int_{-h_f-h_p}^{h_f+h_p} \tau_{\theta z}dz = \int_{-h_f}^{h_f} \tau_{\theta z}^f dz + 2\int_{h_f}^{h_f+h_p} \tau_{\theta z}^p dz \end{aligned} \tag{33}$$

Now, by substituting the stress components in terms of displacement components Eqs. (16)-(20) and Eqs. (28)-(32) in Eqs. (33) and carrying out the integrations, one can obtain the resultant moments and shear force components caused by the stresses as [30]:

$$\begin{aligned} M_{rr} &= \left[\left(d_1+d_2\right)\frac{\partial \psi_r}{\partial r} + \left(\nu d_1 + \frac{\bar{C}_{12}^E}{\bar{C}_{11}^E}d_2\right)\left(\frac{\partial \psi_\theta}{r\partial \theta} + \frac{\psi_r}{r}\right) - \frac{4}{\pi}h_p\bar{e}_{31}\varphi\right] \\ M_{\theta\theta} &= \left[\left(\nu d_1 + \frac{\bar{C}_{12}^E}{\bar{C}_{11}^E}d_2\right)\frac{\partial \psi_r}{\partial r} + \left(d_1+d_2\right)\left(\frac{\partial \psi_\theta}{r\partial \theta} + \frac{\psi_r}{r}\right) - \frac{4}{\pi}h_p\bar{e}_{31}\varphi\right] \\ M_{r\theta} &= \frac{1}{2}\left[\left(\left(1-\nu\right)d_1 + \left(1-\frac{\bar{C}_{12}^E}{\bar{C}_{11}^E}\right)d_2\right)\right]\left(\frac{\partial \psi_r}{r\partial \theta} + \frac{\partial \psi_\theta}{\partial r} - \frac{\psi_\theta}{r}\right) \\ Q_r &= A_3\left(\frac{\partial w}{\partial r} + \psi_r\right) - \frac{4}{\pi}h_p e_{15}\frac{\partial \varphi}{\partial r} \\ Q_\theta &= A_3\left(\frac{\partial w}{r\partial \theta} + \psi_\theta\right) - \frac{4}{\pi}h_p e_{15}\frac{\partial \varphi}{r\partial \theta} \end{aligned} \tag{34}$$

where the coefficients of d_1, d_2 and A_3 in the above equations are related to plate stiffness and are given by

$$d_1 = \int_{-h_f}^{h_f}\frac{z^2E(z)}{1-\nu^2}dz \qquad d_2 = 2\int_{h_f}^{h_f+h_p}\bar{C}_{11}^E z^2 dz$$

$$A_3 = \frac{1}{2}\int_{-h_f}^{h_f}\frac{\kappa^2E(z)}{\left(1+\nu\right)}dz + 2\kappa^2C_{55}^E h_f$$

It is to be noted that M_{rr}, $M_{r\theta}$, $M_{\theta\theta}$, Q_r and Q_θ must satisfy the following dynamic equilibrium equations [31]:

$$\begin{aligned} &\frac{\partial Q_r}{\partial r} + \frac{\partial Q_\theta}{r\partial \theta} + \frac{Q_r}{r} \\ &\quad - \left(\int_{-h_f}^{h_f}\rho_f(z)\frac{\partial^2 u_z}{\partial t^2}dz + 2\int_{h_f}^{h_f+h_p}\rho_p\frac{\partial^2 u_z}{\partial t^2}dz\right) \\ &\quad = 0 \end{aligned} \tag{35}$$

$$\frac{\partial M_{rr}}{\partial r}+\frac{\partial M_{r\theta}}{r\partial\theta}+\frac{M_{rr}-M_{\theta\theta}}{r}-Q_r -\left(\int_{-h_f}^{h_f} z\rho_f(z)\frac{\partial^2 u_r}{\partial t^2}dz+2\int_{h_f}^{h_f+h_p} z\rho_p\frac{\partial^2 u_r}{\partial t^2}dz\right)=0 \quad (36)$$

$$\frac{\partial M_{r\theta}}{\partial r}+\frac{\partial M_{\theta\theta}}{r\partial\theta}+\frac{2M_{r\theta}}{r}-Q_\theta -\left(\int_{-h_f}^{h_f} z\rho_f(z)\frac{\partial^2 u_\theta}{\partial t^2}dz+2\int_{h_f}^{h_f+h_p} z\rho_p\frac{\partial^2 u_\theta}{\partial t^2}dz\right)=0 \quad (37)$$

where ρ_f and ρ_p are material densities of the FGM plate and piezoelectric layer, respectively.

Substituting Eqs. (34) into Eqs. (35)-(37), one can get the equations of motion:

$$A_3(\Delta w+\frac{\partial\psi_r}{\partial r}+\frac{\psi_r}{r}+\frac{\partial\psi_\theta}{r\partial\theta})-A_6\Delta\varphi-A_7\frac{\partial^2 w}{\partial t^2}=0 \quad (38)$$

$$\begin{aligned}&A_1\Delta\psi_r+A_2\frac{\partial}{r\partial r}\left(r\left(\frac{\partial\psi_r}{\partial r}+\frac{\psi_r}{r}+\frac{\partial\psi_\theta}{r\partial\theta}\right)\right)\\&\quad-A_3\left(\psi_r+\frac{\partial w}{\partial r}\right)-(d_1+d_2)\left(\frac{\psi_r}{r^2}+\frac{\partial\psi_\theta}{r^2\partial\theta}\right)\\&-A_2\frac{\partial\psi_r}{r\partial r}-A_1\frac{\partial\psi_\theta}{r^2\partial\theta}+A_5\frac{\partial\varphi}{\partial r}-A_4\frac{\partial^2\psi_r}{\partial t^2}=0\end{aligned} \quad (39)$$

$$\begin{aligned}&A_1\Delta\psi_\theta+A_2\frac{\partial}{r\partial\theta}\left(\frac{\partial\psi_r}{\partial r}+\frac{\psi_r}{r}+\frac{\partial\psi_\theta}{r\partial\theta}\right)\\&\quad-A_3\left(\psi_\theta+\frac{\partial w}{r\partial\theta}\right)+2A_1\left(\frac{\partial\psi_r}{r^2\partial\theta}-\frac{\psi_\theta}{2r^2}\right)\\&+A_5\frac{\partial\varphi}{r\partial\theta}-A_4\frac{\partial^2\psi_\theta}{\partial t^2}=0\end{aligned} \quad (40)$$

where the Laplace operator in polar coordinate system is given by

$$\Delta=\frac{\partial^2}{\partial r^2}+\frac{\partial}{r\partial r}+\frac{\partial^2}{r^2\partial\theta^2}$$

A_1, A_2, A_3, A_4, A_5, A_6 and A_7 are constants governed by material properties and structural geometry, given in Appendix A.

Note that all of the electrical variables primarily must satisfy the Maxwell's equation, which requires that the divergence of the electric flux density vanishes at any point within the media. This condition can be satisfied by enforcing the integration of the electric flux divergence across the thickness of the piezoelectric layers to be zero for any r and θ as [32]:

$$\int_{h_f}^{h_f+h_p}\vec{\nabla}.\vec{D}dz=\int_{h_f}^{h_f+h_p}\left(\frac{\partial(rD_r)}{r\partial r}+\frac{\partial D_\theta}{r\partial\theta}+\frac{\partial D_z}{\partial z}\right)dz=0$$

Now, by substituting Eqs. (25 to 27) into the above equation we arrive at:

$$\begin{aligned}&-\frac{h_p{}^2\bar{\Xi}_{11}}{\pi^2\bar{\Xi}_{33}}\Delta\varphi+\varphi+\frac{h_p{}^2(e_{15}+\bar{e}_{31})}{2\pi\bar{\Xi}_{33}}\left(\frac{\partial\psi_r}{\partial r}+\frac{\psi_r}{r}+\frac{\partial\psi_\theta}{r\partial\theta}\right)\\&+\frac{h_p{}^2e_{15}}{2\pi\bar{\Xi}_{33}}\Delta w=0\end{aligned} \quad (41)$$

5. Solutions method

In the four differential equations of motion, Eqs. (38)-(41), there are four independent variables w, ψ_r,ψ_θ and φ that need to be defined. The solution procedure is described hereafter. Eliminating ψ_r,ψ_θ and φ from Eqs. (38), (39), (40) and (41) yields a decoupled six-order partial differential equation in terms of w only, namely,

$$\begin{aligned}&P_1\Delta\Delta\Delta w+P_2\Delta\Delta w+P_3\Delta\Delta\left(\frac{\partial^2 w}{\partial t^2}\right)+P_4\Delta\left(\frac{\partial^4 w}{\partial t^4}\right)\\&\quad+P_5\Delta\left(\frac{\partial^2 w}{\partial t^2}\right)+P_6\frac{\partial^2 w}{\partial t^2}+P_7\frac{\partial^4 w}{\partial t^4}=0\end{aligned} \quad (42)$$

where the coefficients, P_1, P_2, P_3, P_4, P_5, P_6 and P_7, are given in Appendix B.

To solve Eq. (42) for w we first assume that [28]

$$w(r,\theta,t)=w_1(r)e^{j(m\theta-\omega t)} \quad (43)$$

Substituting Eq. (43) into Eq. (32) and after cancelling the $e^{j(m\theta-\omega t)}$ term one would get:

$$\begin{aligned}&P_1\bar{\Delta}\bar{\Delta}\bar{\Delta}w_1+\left(P_2-P_3\omega^2\right)\bar{\Delta}\bar{\Delta}w_1+\left(P_4\omega^4-P_5\omega^2\right)\bar{\Delta}w_1\\&\quad+\left(P_7\omega^4-P_6\omega^2\right)w_1=0\end{aligned} \quad (44)$$

where $\bar{\Delta}$ is a given by;

$$\bar{\Delta}=\frac{d^2}{dr^2}+\frac{d}{rdr}-\frac{m^2}{r^2}$$

Eq. (44) can be solved by method of decomposition operator and noting that the w_1 is non-singular at the center of the plate; the general solution of Eq. (44) yields

$$w_1(r) = C_{1m}Z_{1m}(\alpha_1 r) + C_{2m}Z_{2m}(\alpha_2 r) + C_{3m}Z_{3m}(\alpha_3 r) \tag{45}$$

where

$$\alpha_1 = \sqrt{|x_1|}\,,\ \alpha_2 = \sqrt{|x_2|}\,,\ \alpha_3 = \sqrt{|x_3|} \tag{46}$$

in which x_1, x_2 and x_3 are the roots of the following cubic characteristic equation,

$$P_1x^3 + (P_2 - P_3\omega^2)x^2 + (P_4\omega^4 - P_5\omega^2)x + P_7\omega^4 - P_6\omega^2 = 0 \tag{47}$$

and

$$Z_{im}(\alpha_i r) = Z_{im}(\alpha_i, r) = \begin{cases} J_m(\alpha_i r) & ,x_i < 0 \\ I_m(\alpha_i r) & ,x_i > 0 \end{cases} (i = 1,2,3) \tag{48}$$

Note that the second type Bessel functions have been omitted from the solution as they become singular at the center of the plate.

Now we assume that the rotations ψ_r and ψ_θ are expressed in terms of the potential functions $\Phi(r,\theta,t)$ and $H(r,\theta,t)$ as

$$\psi_r = \frac{\partial \Phi}{\partial r} + \frac{\partial H}{r\partial \theta}\ \ \psi_\theta = \frac{\partial \Phi}{r\partial \theta} - \frac{\partial H}{\partial r} \tag{49}$$

After substituting the above relations into Eqs. (39) and (40), we get:

$$\frac{\partial}{\partial r}\left[(d_1+d_2)\Delta\Phi - A_3\Phi - A_4\frac{\partial^2\Phi}{\partial t^2} - A_3 w + A_5\varphi\right] + \frac{\partial}{r\partial\theta}\left[A_1\Delta H - A_3 H - A_4\frac{\partial^2 H}{\partial t^2}\right] = 0 \tag{50}$$

$$\frac{\partial}{r\partial\theta}\left[(d_1+d_2)\Delta\Phi - A_3\Phi - A_4\frac{\partial^2\Phi}{\partial t^2} - A_3 w + A_5\varphi\right] - \frac{\partial}{\partial r}\left[A_1\Delta H - A_3 H - A_4\frac{\partial^2 H}{\partial t^2}\right] = 0 \tag{51}$$

By applying the operator $\partial/r\partial\theta$ to Eq. (50), $(1/r + (\partial/r\ \partial r))$ to Eq. (51), and subtracting the results, we obtain a decoupled equation in terms of H,

$$\Delta\left(A_1\Delta H - A_3 H - A_4\frac{\partial^2 H}{\partial t^2}\right) = 0 \tag{52}$$

Similarly, application of the operator $(1/r + (\partial/r\ \partial r))$ to Eq. (50), $\partial/r\ \partial\theta$ to Eq. (51), and adding the results yields another decoupled equation free of H,

$$\Delta\left[(d_1+d_2)\Delta\Phi - A_3\Phi - A_4\frac{\partial^2\Phi}{\partial t^2} - A_3 w + A_5\varphi\right] = 0 \tag{53}$$

It is assumed that Φ, H, and φ take the form

$$\begin{aligned} \Phi(r,\theta,t) &= \hat{\Phi}(r)e^{i(m\theta-\omega t)} \\ H(r,\theta,t) &= \hat{H}(r)e^{i(m\theta-\omega t)} \\ \varphi(r,\theta,t) &= \hat{\varphi}(r)e^{i(m\theta-\omega t)} \end{aligned} \tag{54}$$

where $\hat{\varphi}(r)$, $\hat{\Phi}(r)$, and $\hat{H}(r)$ are amplitudes of $\varphi(r,\theta,t)$, $H(r,\theta,t)$ and $\Phi(r,\theta,t)$, respectively. Substituting Eqs. (43) and (54) into Eqs. (38), (52), (53) and (41) reduces to

$$A_3\bar{\Delta}\hat{\Phi} + A_3\bar{\Delta}w_1 + A_7\omega^2 w_1 - A_6\bar{\Delta}\hat{\varphi} = 0 \tag{55}$$

$$A_1\bar{\Delta}\hat{H} - \left(A_3 - A_4\omega^2\right)\hat{H} = 0 \tag{56}$$

$$\left(d_1+d_2\right)\bar{\Delta}\hat{\Phi} - \left(A_3 - A_4\omega^2\right)\hat{\Phi} - A_3 w_1 + A_5\hat{\varphi} = 0 \tag{57}$$

$$\bar{\Delta}\hat{\Phi} + A_8\bar{\Delta}w_1 - A_9\bar{\Delta}\hat{\varphi} + A_{10}\hat{\varphi} = 0 \tag{58}$$

where the coefficients, A_8, A_9, and A_{10}, are given in Appendix A. Solving Eq. (56) for $\hat{H}$ gives

$$\hat{H}(r) = C_{6a}Z_{6m}(\beta_1 r) + C_{7a}Z_{7m}(\beta_1 r) \tag{59}$$

where C_{6a} and C_{7a} are arbitrary constants and

$$\beta_1 = \sqrt{|F_1|}, \qquad F_1 = \frac{A_3 - A_4\omega^2}{A_1} \tag{60}$$

$$Z_{6m}(\beta_1 r) = \begin{cases} J_m(\beta_1 r), F_1 < 0 \\ I_m(\beta_1 r), F_1 > 0 \end{cases}, \qquad Z_{7m}(\beta_1 r) = \begin{cases} Y_m(\beta_1 r), F_1 < 0 \\ K_m(\beta_1 r), F_1 > 0 \end{cases} \tag{61}$$

To avoid singularity at the center of the plate $C_{7a}=0$. Thus, Eq. (59) is reduced to

$$\hat{H}(r) = C_{6a}Z_{6m}(\beta_1 r) \tag{62}$$

Solving Eqs. (55), (57) and (58) for $\hat{\Phi}$ yields

$$\hat{\Phi}(r)=\chi_1\left\{\frac{G_1\left(A_9A_3-A_6A_8\right)}{A_3-A_4\omega^2}\bar{\Delta}\bar{\Delta}w_1+\left[\frac{A_5\left(A_9A_3-A_6A_8\right)}{G_2}+\frac{G_1\left(A_7A_9\omega^2-A_3A_{10}\right)-A_3}{A_3-A_4\omega^2}-\frac{A_3A_5\left(A_8-1\right)}{\left(A_6-A_3A_9\right)\left(A_3-A_4\omega^2\right)}\right]\bar{\Delta}w_1+\left[\frac{A_5A_9A_7\omega^2-A_6A_{10}A_3}{G_2}-\frac{A_{10}A_3^2+\left(A_{10}d_1+A_{10}d_2-A_5\right)A_7\omega^2}{\left(A_6-A_3A_9\right)\left(A_3-A_4\omega^2\right)}\right]w_1\right\} \quad (63)$$

Substituting Eqs. (45), (54), (62) and (63) into Eq. (49) and replacing iC_{6a} by C_6 yields

$$\psi_r(r,\theta,t)=\left\{\chi_1\sum_{n=1}^{3}\chi_6(x_n)C_n\alpha_nZ'_{nm}(\alpha_nr)+C_6mZ_{6m}(\beta_1r)/r\right\}e^{i(m\theta-\omega t)} \quad (64)$$

$$\psi_\theta(r,\theta,t)=\left\{m\chi_1\sum_{n=1}^{3}\chi_6(x_n)C_nZ_{nm}(\alpha_nr)/r+C_6\beta_1Z'_{6m}(\beta_1r)\right\}e^{i(m\theta-\omega t)} \quad (65)$$

where the coefficients χ_1 and $\chi_6(x_n)$ are given in Appendix C. Substituting Eq. (63) into Eq. (55), $\hat{\varphi}(r)$ yields

$$\hat{\varphi}(r)=-\frac{d_1+d_2}{A_5}\bar{\Delta}\hat{\Phi}(r)+\frac{A_3-A_4\omega^2}{A_5}\hat{\Phi}(r)+\frac{A_3}{A_5}w_1(r) \quad (66)$$

Substituting Eqs. (45), (63) and (66) into Eq. (52) results in

$$\varphi(r,\theta,t)=\sum_{n=1}^{3}\left[\chi_1\chi_6(x_n)(A_3-A_4\omega^2-d_1x_i-d_2x_i)/A_5+A_3/A_5\right]C_nZ_{nm}(\alpha_nr)e^{i(m\theta-\omega t)} \quad (67)$$

5.1 Frequencies determination by boundary conditions

In the preceding sections we obtained explicit expressions for transverse displacement *w (r,θ,t)*, rotations $\psi_r(r,\theta,t)$, $\psi_\theta(r,\theta,t)$, and electric potential $\varphi(r,\theta,t)$, which are all functions of the frequency ω. To determine the frequency, the boundary conditions must be employed. Two kinds of boundary conditions, clamped edge and simply supported edges, are addressed. For simply supported edges, depending upon the in-plane behavior in tangent plane at the edge $r=r_0$, two types: hard type and soft type will be considered. These correspond to the case when the rotation of the boundary edge in the plane tangent to the plate structure's mid-surface, normal to the respective edge (ψ_θ) is either unrestrained (soft type) or completely restrained (hard type).

5.1.1 Clamped edge

For clamped edge at $r=r_0$, both the transverse displacement w and rotations ψ_r and ψ_θ vanish, namely,

$$\begin{aligned}&w(r_0,\theta,t)=0\\&\psi_r(r_0,\theta,t)=0\\&\psi_\theta(r_0,\theta,t)=0\end{aligned} \quad (68)$$

where r_0 is radius of the plate. If the plate is isolated at the edge, the electrical flux conservation equation is given by

$$\int_{h_f}^{h_f+h_p}D_r(r_0,\theta,t)dz=0 \quad (69)$$

Substituting the solutions obtained in the preceding sections for w,ψ_r , ψ_θ and φ into Eqs. (68) and (69) and some simplifications yields

$$\begin{pmatrix}s_{11}^{(a)}&s_{12}^{(a)}&s_{13}^{(a)}&0\\s_{21}^{(a)}&s_{22}^{(a)}&s_{23}^{(a)}&s_{26}^{(a)}\\s_{31}^{(a)}&s_{32}^{(a)}&s_{33}^{(a)}&s_{36}^{(a)}\\s_{41}^{(a)}&s_{42}^{(a)}&s_{43}^{(a)}&0\end{pmatrix}\begin{pmatrix}C_1\\C_2\\C_3\\C_6\end{pmatrix}=\begin{pmatrix}0\\0\\0\\0\end{pmatrix} \quad (70)$$

where $s_{ij}^{(a)}$, $s_{26}^{(a)}$ and $s_{36}^{(a)}$ *(i=1,2,3,4; j=1,2,3)*, are functions of the frequencies, given in Appendix D. Non-trivial solution for C_1, C_2, C_3, and C_6 implies that the determinant of the coefficients matrix of Eq. (70) vanishes, namely,

$$\begin{vmatrix}s_{11}^{(a)}&s_{12}^{(a)}&s_{13}^{(a)}&0\\s_{21}^{(a)}&s_{22}^{(a)}&s_{23}^{(a)}&s_{26}^{(a)}\\s_{31}^{(a)}&s_{32}^{(a)}&s_{33}^{(a)}&s_{36}^{(a)}\\s_{41}^{(a)}&s_{42}^{(a)}&s_{43}^{(a)}&0\end{vmatrix}=0 \quad (71)$$

Solving Eq. (71) for ω gives the frequencies of

flexural free vibrations.

5.1.2 Simply supported edge (hard type)

At the edge $r=r_0$, the transverse displacement w, the resist bending moment in the z–r plane M_{rr}, and the rotation in tangent plane ψ_θ vanish:

$$\begin{aligned} &w(r_0,\theta,t)=0\\ &M_{rr}(r_0,\theta,t)=0\\ &\psi_\theta(r_0,\theta,t)=0 \end{aligned} \tag{72}$$

Of course, Eq. (69) should also be satisfied. If the solutions for w, ψ_r, ψ_θ and φ are substituted into Eqs. (72) and (69), four linear equations in terms of the arbitrary constants, C_1, C_2, C_3, and C_6 are obtained:

$$\begin{pmatrix} s_{11}^{(b)} & s_{12}^{(b)} & s_{13}^{(b)} & 0\\ s_{21}^{(b)} & s_{22}^{(b)} & s_{23}^{(b)} & s_{26}^{(b)}\\ s_{31}^{(b)} & s_{32}^{(b)} & s_{33}^{(b)} & s_{36}^{(b)}\\ s_{41}^{(b)} & s_{42}^{(b)} & s_{43}^{(b)} & s_{46}^{(b)} \end{pmatrix}\begin{pmatrix} C_1\\ C_2\\ C_3\\ C_6 \end{pmatrix}=\begin{pmatrix} 0\\ 0\\ 0\\ 0 \end{pmatrix} \tag{73}$$

where the coefficients, $s_{ij}^{(b)}$, $s_{26}^{(b)}$, $s_{36}^{(b)}$ and $s_{46}^{(b)}$, ($i=1,2,3,4$; $j=1,2,3$), are given in Appendix E. To obtain non-trivial solutions for C_1, C_2, C_3, and C_6, the determinant of the coefficients matrix of Eq. (73) must vanish, from which the frequencies, ω, can be obtained.

5.1.3 Simply supported edge (soft type)

At the edge $r=r_0$, the transverse displacement w, the resist bending moment in the z–r plane and the z–θ plane, M_{rr} and $M_{r\theta}$ (instead of ψ_θ), vanish:

$$\begin{aligned} &w(r_0,\theta,t)=0\\ &M_{rr}(r_0,\theta,t)=0\\ &M_{r\theta}(r_0,\theta,t)=0 \end{aligned} \tag{74}$$

Obviously, Eq. (69) should be satisfied again. If the solutions for w, ψ_r, ψ_θ and φ are substituted into Eqs. (74) and (69), Eq. (73) is obtained again, but the coefficients, $s_{3n}^{(b)}$, $s_{36}^{(b)}$ ($n=1, 2, 3$), are replaced by $s_{3n}^{(c)}$ and $s_{36}^{(c)}$ which are defined in Appendix F. The frequencies, ω, can be obtained again from the condition that the determinant of the coefficients matrix must vanish.

5.2 Mode shapes

It is noted that only three of the four equations in Eqs. (70) and (73) are linearly independent. Thus, C_1, C_2, and C_6 can be expressed in terms of C_3 by solving the first equations of Eqs. (70) and (73), as follows:

$$\begin{aligned} C_1&=C_{C1}C_3\\ C_2&=C_{C2}C_3\\ C_6&=C_{C6}C_3 \end{aligned} \tag{75}$$

where the coefficients, C_{C1}, C_{C2}, and C_{C6}, are given in Appendix G. Substituting Eq. (75) into the solutions for w, ψ_r, ψ_θ and φ, which we obtained in the preceding sections, yields the mode shapes of w, ψ_r, ψ_θ and φ, respectively. The normal modes of the transverse displacement $w_1(r,\theta)$ are given by

$$w_1(r,\theta)=\sum_{n=1}^{3}C_{Cn}Z_{np}(\alpha_n r)\begin{pmatrix}\sin(m\theta)\\ \cos(m\theta)\end{pmatrix} \tag{76}$$

where to get a close form we let $C_{C3}=1$; C_{C1} and C_{C2} are given in Appendix G.

The normal modes of the rotation in the z–r plane are given by

$$\begin{aligned}\psi_r(r,\theta,t)=\Bigg\{&\chi_1\sum_{n=1}^{3}\chi_6(x_n)C_{Cn}Z'_{nm}(\alpha_n r)\\ &+C_{C6}mZ_{6m}(\beta_1 r)/r\Bigg\}\begin{pmatrix}\sin(m\theta)\\ \cos(m\theta)\end{pmatrix}\end{aligned} \tag{77}$$

And the normal modes of the rotation in the tangent plane are given by

$$\begin{aligned}\psi_\theta(r,\theta,t)=\Bigg\{&m\chi_1\sum_{n=1}^{3}\chi_6(x_n)C_{Cn}Z_{nm}(\alpha_n r)/r\\ &+C_{C6}\beta_1 Z'_{6m}(\beta_1 r)\Bigg\}\begin{pmatrix}\cos(m\theta)\\ -\sin(m\theta)\end{pmatrix}\end{aligned} \tag{78}$$

Also the normal modes of the electric potential are given by

$$\begin{aligned}\varphi(r,\theta,t)=\sum_{n=1}^{3}\Big\{\Big(\chi_1\chi_6(x_n)+A_3\Big)\Big/A_5\Big\}\\ C_{Cn}Z_{nm}(\alpha_n r)\begin{pmatrix}\sin(m\theta)\\ \cos(m\theta)\end{pmatrix}\end{aligned} \tag{79}$$

Before going further into the results and discussions, primarily we have to make sure that the obtained results are valid. To do this, initially for some special cases, results are compared with those given in the literature [28].

In the next step, since there were no published results for the compound piezoelectric FGM plate, we decided to verify the validity of obtained results with those of FEM results. Our FEM model for piezo- FG plate is comprised of a 3D 8-noded solid element with: number of total nodes 26950, number of total elements 24276, 3 DOF per node (translation) in the host plate element and 6 DOF per node (3 translation, temperature, voltage and magnetic properties) in the piezoelectric element.

6. Numerical examples and discussion

In order to solve the above relations, in this section, two piezoelectric-bonded FGM plates are considered: a circular plate with clamped boundary condition, and a circular plate with hard type simply-supported boundary condition. The material parameters and geometry of the FGM plate and piezoelectric layers used in the numerical example are listed in Table. 1.

The numerical solution for a three-layer laminated FGM plate shown in Fig. 1 is investigated. The piezoelectric layers are poled in the thickness direction and both surfaces of each layer are short-circuited. The thickness of the FGM layer and piezoelectric layers is 20 and 2mm, respectively. The results are compared with those of FEA and the analytical model [28]. Two kinds of boundary conditions, i.e., clamped edge and simply supported edge, are investigated. Table 2 and Table 3 list comparisons of the frequencies calculated for FGM plate and piezo-FGM plate by the FSDT-based model (proposed), the classical plate theory (CPT)-based model [28] and 3D FEA for clamped edge as well as simply supported edge boundary conditions.

Table 1. Material properties and geometric size of the piezoelectric coupled FGM plate.

Property	FGM Plate	PZT4
E (GPa)	$E_c = 205$	$C_{11}^E = 132$
	$E_m = 200$	$C_{33}^E = 115$
		$C_{12}^E = 71$
		$C_{13}^E = 73$
		$C_{55}^E = 26$
Density (kg/m^3)	ρ_c =8900	7500
	ρ_m =7800	
e31 (C/m^2)		−4.1
e33 (C/m^2)		14.1
e15 (C/m^2)		10.5
Ξ_{11} (nF/m)		7.124
Ξ_{33} (nF/m)		5.841
r_0 (mm)		600
h_f (mm)		10
h_p (mm)		2

As one can see from Tables 2 and 3, the obtained results from the analytical method when g=0 (isotropic steel plate) correspond closely with the results of reference [28] and FEM solution. As seen in these tables, the maximum difference of our solution with FEM is about 4.22% for the simply supported case and 1.50% for the clamped case. This difference can be described in a way that since the clamped edge BC is stiffer than the simply supported edge, it seems that the derived stiffness matrix (K) using variational method results in more accurate answers for clamped BC compared to the simply supported edge BC.

After verification of the results, we start discussing the obtained results from the closed form solution and

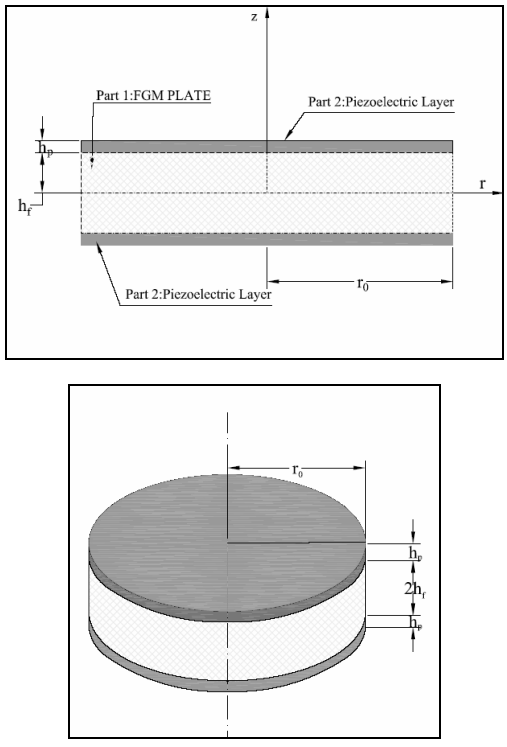

Fig. 1. Schematic representation of the FGM circular plate with two piezoelectric layers mounted on its upper and lower surfaces.

Table 2. Values of the first three resonance frequencies (Hz) for FGM plate and piezo-FGM plate in the case of clamped boundary condition for various values of power index.

Power Index	Mode no.	FGM plate				Coupled Piezo-FGM plate			
g	m	Present FSDPT	Present (FEM)	Difference (%)	Wang et al. [28]	Present FSDPT	Present (FEM)	Difference (%)	Wang et al. [28]
0	0	*138.45*	*139.29*	*0.60*	*138.42*	*143.70*	*144.75*	*0.73*	*143.64*
	1	*288.16*	*289.80*	*0.57*	*288.05*	*299.02*	*300.57*	*0.52*	*298.92*
	2	*472.61*	*473.48*	*0.18*	*472.59*	*490.51*	*492.74*	*0.45*	*490.37*
1	0	*134.68*	*135.47*	*0.58*	-	*140.38*	*142.32*	*1.36*	-
	1	*280.27*	*281.86*	*0.56*	-	*292.14*	*296.04*	*1.32*	-
	2	*459.67*	*460.49*	*0.18*	-	*479.04*	*482.25*	*0.66*	-
3	0	*132.76*	*133.68*	*0.69*	-	*138.67*	*140.71*	*1.45*	-
	1	*276.31*	*278.14*	*0.66*	-	*288.59*	*292.69*	*1.40*	-
	2	*453.17*	*454.42*	*0.28*	-	*473.22*	*476.80*	*0.75*	-
5	0	*132.18*	*133.11*	*0.70*	-	*138.14*	*140.18*	*1.46*	-
	1	*275.08*	*276.95*	*0.68*	-	*287.47*	*291.60*	*1.42*	-
	2	*451.14*	*452.47*	*0.29*	-	*471.39*	*475.03*	*0.77*	-
7	0	*131.91*	*132.83*	*0.69*	-	*137.89*	*139.93*	*1.46*	-
	1	*274.51*	*276.36*	*0.67*	-	*286.95*	*291.07*	*1.41*	-
	2	*450.21*	*451.51*	*0.29*	-	*470.53*	*474.16*	*0.77*	-
9	0	*131.75*	*132.75*	*0.75*	-	*137.75*	*139.85*	*1.50*	-
	1	*274.20*	*276.20*	*0.72*	-	*286.66*	*290.75*	*1.41*	-
	2	*449.68*	*450.90*	*0.27*	-	*470.04*	*473.33*	*0.70*	-
10	0	*131.70*	*132.60*	*0.68*	-	*137.70*	*139.72*	*1.45*	-
	1	*274.08*	*275.89*	*0.66*	-	*286.56*	*290.63*	*1.40*	-
	2	*449.50*	*450.74*	*0.28*	-	*469.89*	*473.45*	*0.75*	-

Table 3. The first three resonance frequencies (Hz) of the FGM plate and piezo FGM-plate in the case of simply supported boundary conditions for different values of power index.

Power Index	Mode no.	FGM plate				Coupled Piezo-FGM plate			
g	m	Present FSDPT	Present (FEM)	Difference (%)	Wang et al. [28]	Present FSDPT	Present (FEM)	Difference (%)	Wang et al. [28]
0	0	*66.88*	*67.27*	*0.57*	-	*69.52*	*72.53*	*4.15*	*69.33*
	1	*188.39*	*189.58*	*0.63*	-	*195.56*	*198.68*	*1.57*	*195.36*
	2	*347.18*	*349.36*	*0.62*	-	*360.26*	*363.16*	*0.80*	*360.08*
1	0	*65.05*	*65.37*	*0.49*	-	*67.88*	*70.81*	*4.14*	-
	1	*183.23*	*184.38*	*0.62*	-	*190.95*	*193.99*	*1.57*	-
	2	*337.60*	*339.78*	*0.64*	-	*351.80*	*354.60*	*0.79*	-
3	0	*64.13*	*64.51*	*0.58*	-	*67.07*	*70.01*	*4.20*	-
	1	*180.63*	*181.95*	*0.72*	-	*188.62*	*191.79*	*1.65*	-
	2	*332.90*	*335.31*	*0.72*	-	*347.52*	*350.58*	*0.87*	-
5	0	*63.84*	*64.23*	*0.60*	-	*66.81*	*69.75*	*4.22*	-
	1	*179.84*	*181.17*	*0.74*	-	*187.92*	*191.08*	*1.65*	-
	2	*331.41*	*333.87*	*0.74*	-	*346.17*	*349.29*	*0.89*	-
7	0	*63.71*	*64.09*	*0.59*	-	*66.72*	*69.62*	*4.17*	-
	1	*179.46*	*180.79*	*0.74*	-	*187.57*	*190.73*	*1.66*	-
	2	*330.72*	*333.15*	*0.73*	-	*345.55*	*348.64*	*0.89*	-
9	0	*63.64*	*64.01*	*0.57*	-	*66.61*	*69.48*	*4.13*	-
	1	*179.24*	*180.55*	*0.72*	-	*187.38*	*190.55*	*1.66*	-
	2	*330.34*	*332.82*	*0.75*	-	*345.20*	*348.38*	*0.91*	-
10	0	*63.62*	*63.99*	*0.57*	-	*66.59*	*69.52*	*4.22*	-
	1	*179.18*	*180.48*	*0.72*	-	*187.32*	*190.45*	*1.64*	-
	2	*330.21*	*332.59*	*0.72*	-	*345.07*	*348.12*	*0.88*	-

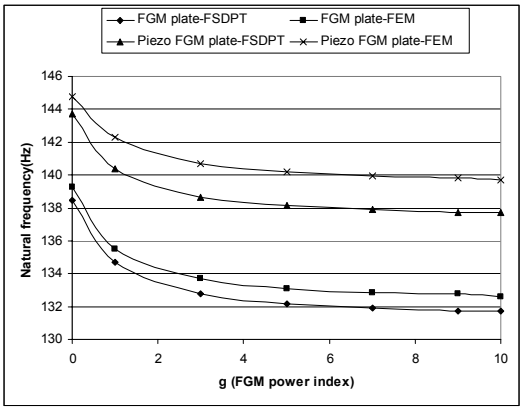

Fig. 2. Effect of power index on the natural frequency for the case of clamped boundary condition (first mode).

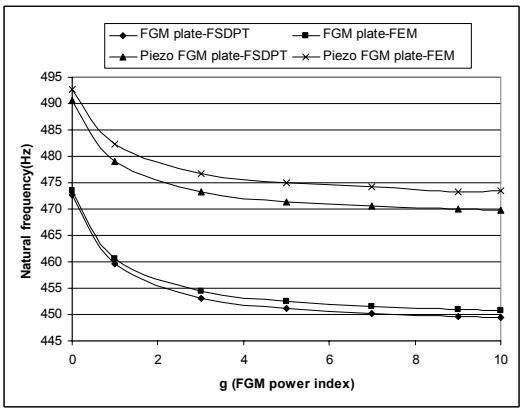

Fig. 3. Effect of power index on the natural frequency for the case of clamped boundary condition (third mode).

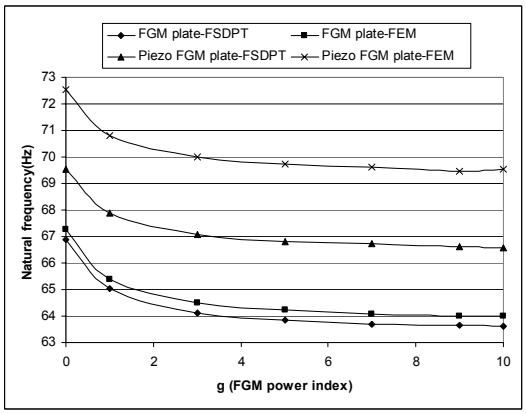

Fig. 4. Effect of power index on the natural frequency for the case of simply supported boundary condition (first mode).

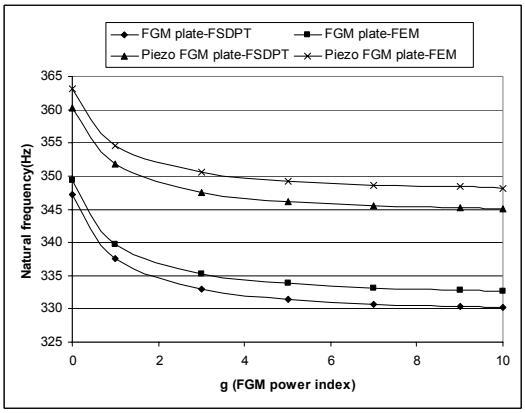

Fig. 5. Effect of power index on the natural frequency for the case of simply supported boundary condition (third mode).

the FEM results. A close inspection of the results listed in Tables 2 and 3 indicates that the amount of difference between analytical and FEM results for the natural frequencies in FGM plate alone in the all vibration modes and for all values of k are less than similar results for the compound plate.

In the next step we try to investigate the effect of FGM power index (g) on the natural frequencies of the compound plate. The obtained results in this table indicate that by increasing the value of k, the frequency of system decreases for both types of boundary conditions in all different vibrational modes. Moreover, this decreasing trend of frequency for smaller values of g is more pronounced; for example, in the case of clamped plate by increasing the value of g from 1 to 3) about 200%) the frequency of the first mode for the compound plate decreases by 1.23%, but by increasing g from 3 to 9 (about 200%) of the same plate and for the same mode, the frequency decreases by 0.66%. It is also observed that for the FGM plate in the case of simply supported boundary condition by increasing g from 0 to 3 the frequency decreases in the third mode of vibration about 4.12%, but by increasing g from 5 to 10, the frequency decreases for the same plate and the same mode about 0.36%. In order to see better the effect of g variations on the natural frequencies of the different plates, Figs. 2 to 5 also illustrate these variations only for the first and third mode shapes.

As seen from Figs. 2 to 5, the behavior of the system follows the same trend in all different cases, i.e., the natural frequencies of the system decrease by increasing of g and stabilizes for g values greater than

7. In fact, for $g >> 1$ the FGM plate becomes a Nickel plate and the compound plate transforms into a laminated plate with metal core as a host plate.

7. Conclusion

In this paper an analytical solution for free flexural vibration of a three-layered piezoelectric laminated FGM circular moderately thick plate is proposed based on Mindlin's first order shear deformation plate theory for the cases where the electrodes on the piezoelectric layers are shortly connected. The material properties of the functionally graded substrate plate are assumed to be graded in the thickness direction according to the power-law distribution in terms of the volume fractions of the constituents, and the electric potential distribution across thickness of piezoelectric layers is modeled by a sinusoidal function and the Maxwell equation is satisfied. The detailed mathematical derivations are presented. Emphasis is placed on investigating the effect of varying the gradient index of FG plate on the free vibration characteristics of the structure. The validity of the obtained results for some specific cases was crossed checked with other references as well as by obtained results from FEM solutions. It is further shown that for vibrating circular compound plates with specified dimensions, one can select a specific piezo-FGM plate that can fulfill the designated natural frequency.

Acknowledgments

This research was funded by the research deputy of the University of Tehran (Project No. 8106002/6/02).

Nomenclature

r_0	:	Plate radius
t	:	Time
c_{ij}	:	Matrix of modulus of elasticity
u_r, u_θ,uz	:	Radial ,circumferential, transverse displacements
$\bar{C}_{ij}^{E}$	:	Components of the symmetric piezoelectric stiffness matrix
V_c ,V_m,	:	Volume fraction of the ceramic and metallic part
D_i	:	Electric displacement components
w	:	Transverse displacement of the mid-plane
e	:	Permeability constant of piezoelectric material
Δ, $\vec{\nabla}$	:	Laplace & Gradient operators in polar coordinate
$\bar{e}$	:	Reduced permeability constant of piezoelectric material
ε , γ	:	Membrane and bending strains
E	:	Young's modulus
φ	:	Electric potential on the mid-surface of the piezoelectric layer
E_k	:	Electric field components
ρ_f ,ρ_p	:	FGM & piezoelectric mass density
g	:	Volume fraction index
σ_i	:	Stress components
k	:	Mindlin's shear factor
υ	:	Poisson's ratio
h_p , $2h_f$	:	Thickness of FG & piezo plate
ω	:	Natural angular frequency
I_m, K_m	:	Modified first kind and the second kind of Bessel functions
Ξ_{33} , Ξ_{11}	:	Dielectric constants (permittivity) of piezoelectric layer
J_m ,Y_m	:	First kind and the second kind of Bessel functions
$\bar{\Xi}_{11}$, $\bar{\Xi}_{33}$	:	Symmetric reduced dielectric constants
m	:	Wave number in circumferential direction
ψ_r ,ψ_θ	:	Rotations of vertical lines perpendicular to the mid-plane,
M_{ij},Q_i	:	Moments & shear force components

Superscript

f, p	:	The variable in FGM & Piezo layer
r, θ, z	:	Radial, circumferential & transverse direction

Subscript

m, c	:	Metal & ceramic

References

[1] M. Koizumi, The concept of FGM, *Ceram. Trans. Func. Grad. Mater.,* 34 (1993) 3-10.

[2] M. Teymur, N. R. Chitkara, K. Yohngjo, J. Aboudi, M. J. Pindera and S. M. Arnold, Thermoelastic Theory for the Response of Materials Functionally Graded in Two Directions, *Int. J. Solids Struct.,* 33 (1996) 931-66.

[3] E. Feldman and J. Aboudi, Buckling analysis of functionally graded plates subjected to uniaxial

loading, *Compos. Struct.,* 38 (1997) 29-36.

[4] Yang and H. S. Shen, Dynamic response of initially stressed functionally graded rectangular thin plates, *Compos. Struct.,* 54 (2001) 497-508.

[5] H. S. Shen, Nonlinear bending response of functionally graded plates subjected to transverse loads and in thermal environments, *Int. J. Mech. Sci.,* 44 (2002) 561-584.

[6] T. Bailey and J. E. Hubbard, Distributed piezoelectric polymer active vibration control of a cantilever beam, *J. Guidance, Control Dyn.,* 8 (1985) 605-611.

[7] F. Peng, A. Ng and Y. R., Hu, Actuator placement optimization and adaptive vibration control of plate smart structures, *J. Intell Mater Syst Struct.,* 16 (2005) 263-271.

[8] W. J. Spencer, W. T. Corbett, L. R. Dominguez and B. D. Shafer, An electronically controlled piezoelectric insulin pump and valves, *IEEE Trans. Sonics Ultrason.,* 25 (1978) 153-156.

[9] S. Dong, X. Du, P. Bouchilloux and K. Uchino, Piezoelectric ring-morph actuation for valve application, *J. Electroceram.,* 8 (2002) 155-161.

[10] C. Y. K. Chee, L. Tong and G. P. Steve, A review on the modelling of piezoelectric sensors and actuators incorporated in intelligent structures, *J. Intel. Mater. Syst. Str.,* 9 (1998) 3-19.

[11] L. Cao, S. Mantell and D. Polla, Design and simulation of an implantable medical drug delivery system using microelectromechanical systems technology, *Sensors Actuators A,* 94 (2001) 117-125.

[12] X. Chen, C. H. J. Fox and S. McWilliam, Optimization of a cantilever microswitch with piezoelectric actuation, *J. Intel. Mater. Syst. Str.,* 15 (2004) 823-834.

[13] Y. Ootao and Y. Tanigawa, Control of transient thermoelastic displacement of a functionally graded rectangular plate bonded to a piezoelectric plate due to nonuniform heating, *Acta Mech.,* 148 (2001) 17-33.

[14] J. N. Reddy and Z. Q. Cheng, Three-dimensional solutions of smart functionally graded plates, *ASME J. Appl. Mech*., 68 (2001) 234-241.

[15] B. L. Wang and N. Noda, Design of smart functionally graded thermo-piezoelectric composite structure, *Smart Mater. Struct.,* 10 (2001) 189-193.

[16] X. Q. He, T. Y. Ng, S. Sivashanker and K. M. Liew, Active control of FGM plates with integrated piezoelectric sensors and actuators, *Int. J. Solids Struct.,* 38 (2001) 1641-1655.

[17] J. Yang, S. Kitipornchai and K. M. Liew, Nonlinear analysis of thermo-electro-mechanical behavior of shear deformable FGM plates with piezoelectric actuators, *Int. J. Numer. Methods Eng.,* 59 (2004) 1605-1632

[18] J. Yang, S. Kitipornchai and K. M. Liew, Large amplitude vibration of thermo-electric-mechanically stressed FGM laminated plates, *Computer Methods in Applied Mechanics and Engineering,* 192, (2003) 3861-3885.

[19] X. L. Huang and H. S. Shen, Vibration and dynamic response of functionally graded plates with piezoelectric actuators in thermal environments, *J. Sound Vib.,* 289 (2006) 25-53.

[20] F. Ebrahimi and A. Rastgoo, An analytical study on the free vibration of smart circular thin FGM plate based on classical plate theory, *Thin-Walled Structures (*2008) Article in press *DOI:* 10.1016/ j.tws.2008.03.008.

[21] F. Ebrahimi and A. Rastgoo, Free vibration analysis of smart annular FGM plates integrated with piezoelectric layers, *Smart Mater. Struct.,* 17 (2008) no. 015044.

[22] A. J. Markworth, K. S. Ramesh and Jr. Parks, Modeling studies applied to functionally graded materials, *J. Mater. Sci.,* 30 (1995) 2183-2193.

[23] J. N. Reddy and G. N. Praveen, Nonlinear transient thermoelastic analysis of functionally graded ceramic-metal plate, *Int. J. Solids Struct*., 35 (1998) 4457-4476.

[24] R. C. Wetherhold and S. Wang, The use of functionally graded materials to eliminate or thermal deformation, *Composite Sci. Tech*., 56 (1996) 1099-1104.

[25] Y. Tanigawa, H. Morishita and S. Ogaki, Derivation of system of fundamental equations for a three dimensional thermoelastic field with nonhomogeneous material properties and its application to a semi infinite body, *J. Thermal Stress,* 22 (1999) 689-711.

[26] H. F. Tiersten, Linear piezoelectric plate vibrations, plenum press, New York, USA, (1969).

[27] D. O. Brush and B. O. Almroth, Buckling of bars plates and shells, McGraw-Hill, New York, USA, (1975).

[28] Q. Wang, S. T. Quek and X. Liu, Analysis of piezoelectric coupled circular plate, *Smart Mater Struct*., 10 (2001) 229-239.

[29] R. D. Mindlin, Influence of rotary inertia and shear on flexural motions of isotropic elastic plates, *J. Appl Mech*., 18 (1951) 31-38.

[30] J. N. Reddy, Theory and analysis of elastic plates, Taylor and Francis, Philadelphia, USA, (1999).

[31] X. Liu, Q. Wang and S. T. Quek, Analytical solution for free vibration of piezoelectric coupled mod-

erately thick circular plates, *Int. J. Solids Struct*., 39 (2002) 2129-2151.

[32] D. Halliday and R. Resnick, Physics, John Wiley and Sons, New York, USA, (1978).

Appendices

Some coefficients referred to in this paper are given as follows:

$$A_1=\frac{1}{2}\left[\left((1-\nu)d_1+\left(1-\frac{\bar{C}_{12}^E}{\bar{C}_{11}^E}\right)d_2\right)\right],$$

$$A_2=\frac{1}{2}\left[\left((1+\nu)d_1+\left(1+\frac{\bar{C}_{12}^E}{\bar{C}_{11}^E}\right)d_2\right)\right],$$

$$A_3=\frac{1}{2}\int_{-h_f}^{h_f}\frac{k^2E(z)}{(1+\nu)}dz+2k^2C_{55}^E h_f,$$

$$A_4=\int_{-h_f}^{h_f}z^2\rho_f(z)dz+2h_p\left(h_f^2+h_fh_p+\frac{1}{3}h_p^2\right)\rho_p$$

$$A_5=\frac{4h_p(e_{31}-\bar{e}_{31}^E)}{\pi},\quad A_6=\frac{4h_pe_{15}}{\pi},$$

$$A_7=\int_{-h_f}^{h_f}\rho_f(z)dz+2h_p\rho_p$$

$$A_8=\frac{e_{15}}{e_{15}+\bar{e}_{31}},\quad A_9=\frac{2\bar{\Xi}_{11}}{\pi(e_{15}+\bar{e}_{31})},$$

$$A_{10}=\frac{2\pi\,\bar{\Xi}_{33}}{h_p^2(e_{15}+\bar{e}_{31})} \tag{A}$$

$$P_1=(d_1+d_2)\left(2h_pe_{15}^2-\bar{\Xi}_{11}A_3\right),$$

$$P_2=A_3\left[2h_p\bar{e}_{31}^2+\frac{\pi^2\bar{\Xi}_{33}(d_1+d_2)}{h_p^{\,2}}\right],$$

$$P_3=A_4(A_3\bar{\Xi}_{11}-2h_pe_{15}^2)+A_7\bar{\Xi}_{11}(d_1+d_2),$$

$$P_4=-A_7A_4\bar{\Xi}_{11},\ P_7=\frac{\pi^2A_7A_4\bar{\Xi}_{33}}{h_p^2}$$

$$P_5=2A_7h_p\left(e_{15}^2-\bar{e}_{31}^2\right)-\frac{\left[A_7(d_1+d_2)+A_4A_3\right]\pi^2\bar{\Xi}_{33}}{h_p^2},$$
$$-A_7A_3\bar{\Xi}_{11}$$

$$P_6=\frac{\pi^2A_7A_3\bar{\Xi}_{33}}{h_p^2}, \tag{B}$$

$$G_1=\frac{(d_1+d_2)}{(A_6-A_3A_9)},\ G_2=A_5\left(A_9A_3-A_6\right)+A_6A_{10}\left(d_1+d_2\right)$$

$$\chi_1=G_2\Big/\left[A_{10}(A_{10}A_3A_6G_1-A_3A_5+A_3A_6-A_4A_6\omega^2)\right]$$

$$\chi_2(x_n)=\frac{G_1(A_9A_3-A_6A_8)x_n^2+(G_1A_7A_9\omega^2-G_1A_3A_{10}-A_3)x_n}{A_3-A_4\omega^2}$$

$$\chi_3(x_n)=\left[A_5(A_9A_3-A_6A_8)x_n\right.$$
$$\left.+A_5A_9A_7\omega^2-A_6A_{10}A_3\right]\Big/G_2$$

$$\chi_4(x_n)=$$
$$\frac{A_3A_5(A_8-1)x_n+A_{10}A_3^2+(A_{10}d_1+A_{10}d_2-A_5)A_7\omega^2}{(A_6-A_3A_9)(A_3-A_4\omega^2)}$$

$$\chi_5(x_n)=\left(d_1x_n+d_2x_n-A_3+A_4\omega^2\right),$$

$$\chi_6(x_n)=\chi_2(x_n)+\chi_3(x_n)-\chi_4(x_n) \tag{C}$$

$$S_{1n}^{(a)}=Z_{nm}(\alpha_nr_0)\ ,$$

$$S_{26}^{(a)}=mZ_{6m}(\beta_1r_0)/r_0\ ,\ S_{36}^{(a)}=\beta_1Z'_{6m}(\beta_1r_0)$$

$$S_{2n}^{(a)}=\chi_1\chi_6(x_n)\alpha_nZ'_{nm}(\alpha_nr_0),$$

$$S_{3n}^{(a)}=m\chi_1\chi_6(x_n)\alpha_nZ_{nm}(\alpha_nr_0)/r_0 \tag{D}$$

$$S_{1n}^{(b)}=Z_{nm}(\alpha_nr_0)\ ,$$

$$S_{26}^{(b)}=2m\left(\beta_1Z'_{6m}(\beta_1r_0)\Big/r_0-Z_{6m}(\beta_1r_0)\Big/r_0^2\right),$$

$$S_{36}^{(b)}=\beta_1Z'_{6m}(\beta_1r_0)$$

$$S_{2n}^{(b)}=\chi_1\chi_6(x_n)\times$$
$$\times\left[\frac{2A_1m^2}{r_0^2}Z_{nm}(\alpha_nr_0)+\right.$$
$$\frac{e_{15}(A_1+A_2)x_n-\bar{e}_{31}(A_3-A_4\omega^2)}{e_{15}-\bar{e}_{31}}Z_{nm}(\alpha_nr_0)-$$
$$\left.\frac{2A_1\alpha_n}{r_0}Z'_{nm}(\alpha_nr_0)\right]-\frac{A_3\bar{e}_{31}}{e_{15}-\bar{e}_{31}}Z_{nm}(\alpha_nr_0)$$

$$S_{3n}^{(b)}=m\chi_1\chi_6(x_n)\times Z_{nm}(\alpha_nr_0)/r_0\ ,$$

$$S_{4n}^{(b)}=\left\{\chi_1\chi_6(x_n)\left(\frac{2\bar{\Xi}_{11}\chi_5}{\pi e_{15}A_5}+1\right)-\frac{2\bar{\Xi}_{11}A_3}{\pi e_{15}A_5}+1\right\}$$
$$\alpha_nZ'_{nm}(\alpha_nr_0)$$

$$S_{46}^{(b)}=mZ_{6m}(\beta_1r_0)/r_0\ ,\ (n=1,\ 2,\ 3) \tag{E}$$

$$S_{3n}^{(c)}=2m\chi_1\chi_6(x_n)$$
$$\times\left(\alpha_nZ'_{nm}(\alpha_nr_0)/r_0-Z_{nm}(\alpha_nr_0)/r_0^2\right)$$

$$S_{36}^{(c)}=-F_1Z_{6m}(\beta_1r_0)+2\beta_1^2Z''_{6m}(\beta_1r_0)\ ,\ (n=1,\ 2,\ 3) \tag{F}$$

$$C_{C1}=\frac{s_{13}s_{26}s_{32}-s_{12}s_{26}s_{33}-s_{13}s_{22}s_{36}+s_{12}s_{23}s_{36}}{s_{12}s_{26}s_{31}-s_{11}s_{26}s_{32}-s_{12}s_{21}s_{36}+s_{11}s_{22}s_{36}},$$

$$C_{C2}=\frac{s_{11}s_{26}s_{33}-s_{13}s_{26}s_{31}-s_{13}s_{21}s_{36}+s_{11}s_{23}s_{36}}{s_{12}s_{26}s_{31}-s_{11}s_{26}s_{32}-s_{12}s_{21}s_{36}+s_{11}s_{22}s_{36}}$$

$$C_{C3}=$$
$$\frac{s_{13}s_{22}s_{31}-s_{12}s_{23}s_{31}-s_{13}s_{21}s_{32}+s_{11}s_{23}s_{32}+s_{12}s_{21}s_{33}-s_{11}s_{22}s_{33}}{s_{12}s_{26}s_{31}-s_{11}s_{26}s_{32}-s_{12}s_{21}s_{36}+s_{11}s_{22}s_{36}} \tag{G}$$